

Crystalline Co-Assemblies of Functional Fullerenes in Methanol with Enhanced Charge Transport

Jianyuan Zhang,[†] Chang-Zhi Li,[†] Spencer T. Williams,[†] Shengqiang Liu,[†] Ting Zhao,[†] and Alex K.-Y. Jen^{*,†,‡}

[†]Department of Materials Science and Engineering and [‡]Department of Chemistry, University of Washington, Seattle, Washington 98195, United States

S Supporting Information

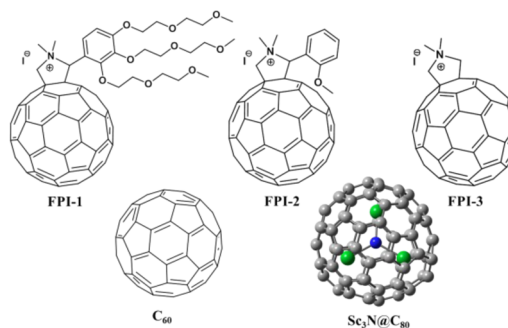
ABSTRACT: Supramolecular arrangement of conjugated molecules has crucial influence on their material properties. For fullerenes and metallofullerenes, tight and ordered packing is beneficial for intermolecular charge transport and energy transfer, but it is tricky to achieve, especially for functionalized cages due to the often extensive solvation and steric effects of functional groups. In this study, we use an amphiphilic fullerene derivative soluble in methanol to form co-assemblies with insoluble fullerene derivatives, pristine fullerene, and metallofullerene via strong $\pi-\pi$ interactions. These mixtures are processable in methanol and show fullerene-templated crystalline structures in spin-cast films. Devices are successfully fabricated on a field-effect transistor platform with this approach, and all co-assemblies show metallic-like conductive properties with significantly enhanced conductivity compared to the pure amphiphilic fullerene derivative.

Fullerenes¹ and metallofullerenes² possess spherical sp^2 conjugated carbon cages that lead to unique optical and electronic properties.³⁻⁵ For example, methano-fullerene derivatives form the cornerstone of high-efficiency organic solar cells as hitherto the best electron acceptors.⁶⁻⁸ As directing the supramolecular arrangement of conjugated molecules is a powerful approach to tune their optoelectronic properties,^{9,10} its utility should not be underestimated even in the context of seemingly isotropic spherical fullerenes. For pristine fullerenes, careful maneuvering their microscopic arrangements may significantly alter their macroscopic properties.^{11,12} Meanwhile, structural design of fullerene derivatives, either by controlling molecular shape¹³⁻¹⁷ or introducing functional groups, can achieve special supramolecular architectures.¹⁸⁻²² In the latter, the concept of amphiphile has been broadly applied, as demonstrated in a very recent work by Nakanishi et al. showing the assembly and co-assembly of pristine and derivatized fullerenes by utilizing the amphiphilic behavior of alkylated fullerenes.²³

Due to the hydrophobic nature of fullerene cage, a key challenge in the application of fullerenes and metallofullerenes is to process them in polar solvents such as alcohols and water, which allows eco-friendly solvent choices, orthogonal-solvent processing in multilayer devices, and biomedical applications. To enable solvation in polar solvents, functionalization with one large or multiple smaller hydrophilic groups is generally

required.²⁴ However, the former sterically prevents cage-to-cage contact, while the latter significantly reduces the conjugation over the fullerene cage; therefore, these methods have limited efficacy in applications where $\pi-\pi$ interactions are essential, such as optoelectronic devices. We believe exploiting non-covalent interactions is an effective alternative approach. Our hypothesis is that amphiphilic fullerene derivatives can stabilize insoluble fullerene-based molecules in solution by strong intermolecular $\pi-\pi$ interactions via tightly packed co-assembly and thereby become amenable to processing in alcohol or water. Herein, we report the use of an amphiphilic fullerene derivative, fulleropyrrolidinium iodide (FPI) FPI-1²⁵ as a surfactant to process insoluble fullerene derivatives, fullerene C_{60} , and metallofullerene $Sc_3N@C_{80}$ ²⁶ (Chart 1) in methanol.

Chart 1. Structures of the Fullerene Derivatives, Fullerene, and Metallofullerene Used in This Study



In addition, we show that films can be deposited via facile spin-coating process. Transmission electron microscopy (TEM) studies reveal that in each case the amphiphile and insoluble content form crystalline co-assemblies. We further demonstrate devices fabricated with these mixtures on a field-effect transistor (FET) platform which show significantly enhanced charge transport in all co-assemblies.

The surfactant FPI-1 is a methanol-soluble amphiphilic molecule, and its thin films have a conductive character caused by an n-doping mechanism. The conductivity of FPI-1 (0.020 S/cm) is one of the highest among solution-processable fullerene derivatives.²⁷ In addition, it was demonstrated that blending FPI-1 with semiconducting phenyl- C_{61} butyric methyl

Received: November 6, 2014

Published: January 30, 2015

ester (PCBM) can further enhance conductivity to 0.032 S/cm,²⁷ and we ascribe the increased conductivity to tighter intermolecular packing as a result of reduced steric effects.²⁷ In the same vein, we have synthesized two considerably smaller analogues of FPI-1 (FPI-2 and FPI-3, Chart 1) with similar procedures²⁸ (Scheme S1) to induce tighter packing compared to pure FPI-1. FPI-2 and FPI-3 are insoluble in methanol or other common organic solvents such as chloroform, chlorobenzene, or toluene. Moreover, we also study pristine fullerene C₆₀ and metallofullerene Sc₃N@C₈₀ for smaller size and better electron transport.

We first verified the amphiphilic behavior of FPI-1 by studying its thin films spin-coated from *o*-xylene, chloroform, and methanol with atomic force microscopy (AFM). Although *o*-xylene and chloroform have affinities to different parts of FPI-1, random intermolecular arrangements are suggested as homogeneous films were observed in both cases (Figure 1a,

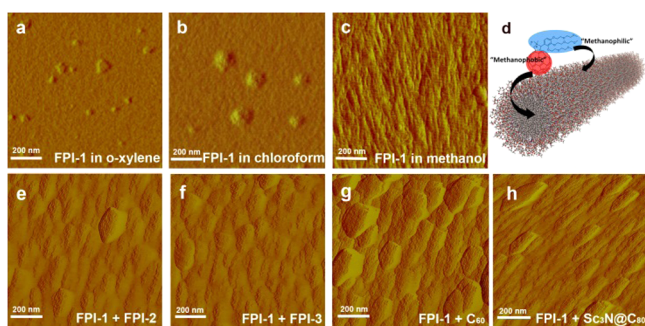


Figure 1. AFM phase images for the thin film deposited from 5 mg/mL FPI-1 solution in (a) *o*-xylene; (b) chloroform; (c) methanol, and (d) schematic representation for proposed assembly structure of FPI-1 in methanol. The AFM images of the mixtures are shown in (e) M1, (f) M2, (g) M3, and (h) M4.

b). On the contrary, the morphology of the film deposited from methanol solution (Figure 1c) shows a distinct tubular microstructure. Clearly, the drastic difference in solvent affinity of the solvophobic cage and the solvophilic chain drives FPI-1 molecules to self-assemble to maximize solvation and minimize fullerene cage exposure to methanol (Figure 1d). Width of the tubular structures was estimated between 20 and 100 nm, consistent with results from amphiphilic C₆₀ derivatives reported by Tour,²⁹ Guldi,³⁰ Aida,³¹ and Martín³² et al.

The mixtures of FPI-1 and an insoluble second content, FPI-2, FPI-3, C₆₀, or Sc₃N@C₈₀, were prepared (Figure S1) in a 4:1 molar ratio, defined as mixtures M1, M2, M3, and M4, respectively. These mixtures were suspended in methanol by extensive sonication (experimental procedure see SI), and dynamic light scattering (DLS) data (Figure S2) of diluted dispersions revealed large aggregates. Immediately after sonication, the solutions were deposited on glass substrates via spin-coating. We note that 20 mol % of the second content completely changes film morphology (Figure 1e–h) compared to pure FPI-1 deposited from the same solvent (Figure 1c). In M1, M2, and M3 (Figure 1e–g), fullerene cages form plate-like structures, instead of tubular structures, in accordance with the reduction of solvophilic chains and increase in solvophobic fullerene cages. In the case of M4 (Figure 1h), bar-like structures, which can be viewed as an intermediate case between the tubular and plate-like structures, are observed, indicating that the Sc₃N@C₈₀, with an alternative ionic

expression form of Sc₃N⁶⁺@C₈₀⁶⁻, may be less repulsive to methanol.

To understand the nature of packing in each self-assembled unit at a molecular level, we studied the films with TEM for high-resolution bright-field imaging and select area electron diffraction (SAED) analysis (Figure 2). In the pure FPI-1 film (Figure 2a) there is no coherent crystalline structure. In each fullerene mixture (Figure 2b–e), however, there is unique crystalline orders, which is direct proof that in these aggregates fullerene cages closely pack together for increased π – π interaction. The size of the crystalline domain is on the order of several hundred nanometers, which is consistent with the DLS results. Meanwhile, the film thickness of 25–40 nm given by AFM and the SAED patterns in TEM strongly suggest the co-assemblies are lamellar, which has been found in similar systems.^{23,33} We note that all structures in Figure 2b–e are more or less derivatives of the packing, symmetry, and orientation natural to unfunctionalized C₆₀,^{11,34} meaning that C₆₀ (also C₈₀ in M4) cages provided the structural template for the assemblies. Figure 2f is an expansion of a 10 × 10 nm area in Figure 2e which more clearly shows highly ordered fullerene arrays, as can be seen in all co-assemblies (Figure S3).

SAED insets in Figure 2b–e show that the functionality in each mixture alters the basic symmetry inherent to the (111) plane in the face-centered cubic (fcc) lattice of C₆₀ in unique ways. All co-assemblies (Figure 2b–e) showed single-crystal-like SAED patterns. In M1 (Figure 2b), diffraction signals corresponding to (110) and (220) lattice spacings of the C₆₀ fcc lattice are visible, but the symmetry of (111) plane of C₆₀ is lost which suggests that the relatively bulky functional group in FPI-2 interferes with the templating influence of the fullerene cage, in addition to the functional group on FPI-1. In contrast, the reduced steric bulk of FPI-3 in M2 (Figure 2c) allows intimate fullerene packing in almost the exact lateral structure as the (111) plane in pure fcc C₆₀. M3 (Figure 2d) is quite similar in structure, but the linear and discrete spread of diffraction signals along the (110) direction is an indication of the formation of an ordered mixture (Figure 2d inset). This inhomogeneity may be due to the greater solvophobicity of C₆₀ compared to FPI-2 and FPI-3. Finally, M4 (Figure 2e) is a disordered co-assembly with the same lateral structure as the (111) plane of bare C₆₀, but diffraction signals are wide and blurry rather than sharp as in M2 indicating a larger defect concentration (Figure 2e). These defects may take the form of local changes in characteristic spacings from inhomogeneities in the distribution of constituent fullerenes, as well as vacancies, and the resulting distortions. We ascribe higher defect concentration unique to M4 to the cooperative templating effects of the C₆₀ cage in FPI-1 and the metallofullerene cage in Sc₃N@C₈₀.

Despite of the unique characteristics in each co-assembly, we find the spacing between their (110) planes (Figure 2g) to be comparable (~1 nm), consistent with the observation that C₆₀ cage templates crystalline structures in all mixtures (in M4 the spacing is a range due to the influence of Sc₃N@C₈₀). Based on this, a schematic drawing of the co-assemblies is shown in Figure 2h. From the TEM bright-field imaging and SAED results, it can be deduced that fullerene cages largely pack as they do in the (111) plane of fcc C₆₀ (with deviations in unique ways), with the cages preferably packing inward and functional groups preferably pointing outward given appropriate stoichiometry and processing, although current data do not exclude other multilayer structures.

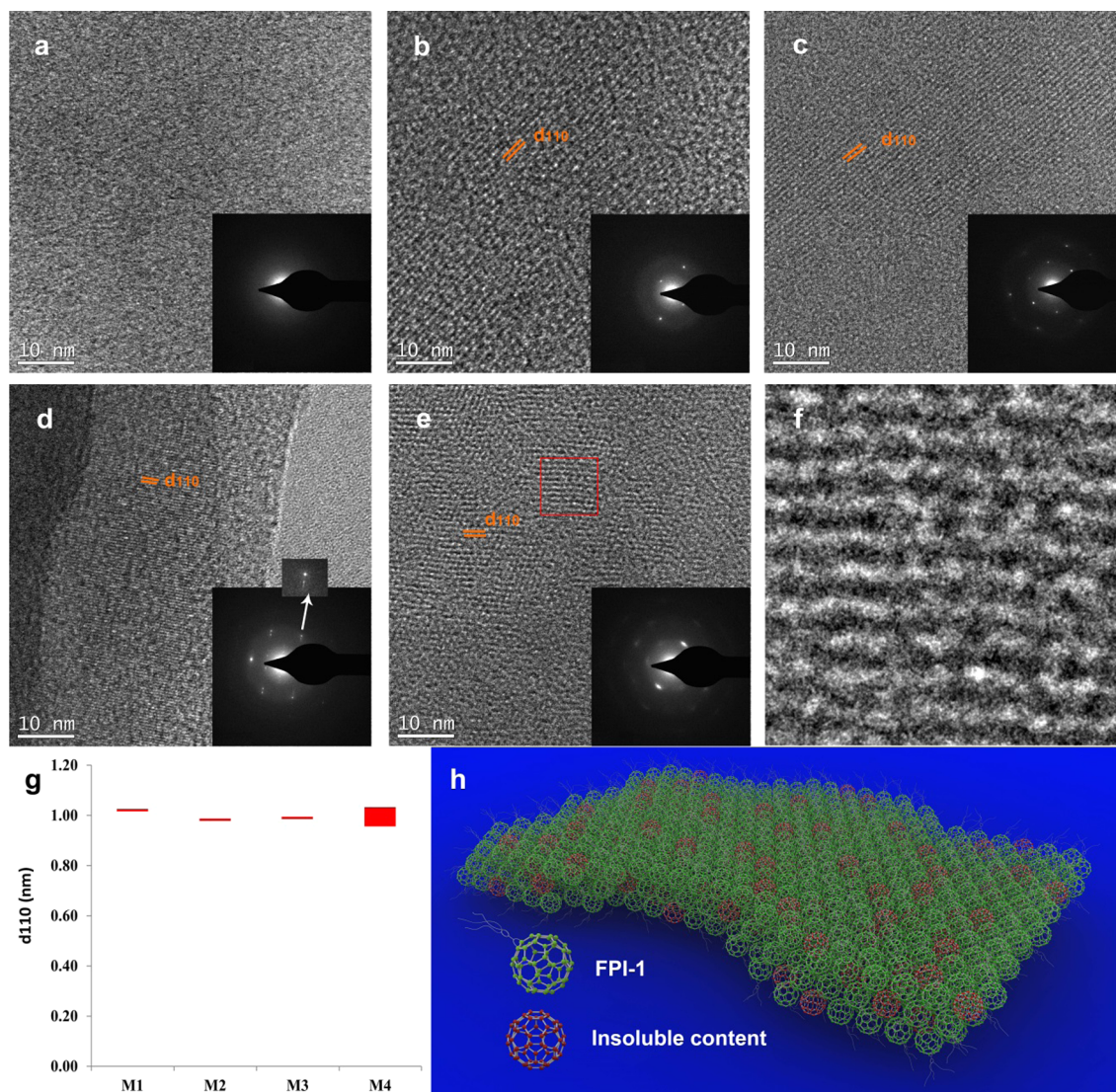


Figure 2. TEM images of films deposited from methanol. (a) FPI-1; (b) M1; (c) M2; (d) M3; (e) M4; (f) expanded image of the 10 × 10 nm red box in (e). (g) (110) spacing values for the mixtures derived from the SAED results shown in b–e. (h) schematic drawing of the crystalline co-assembly. Insets in b–e: SAED images.

As an important parameter for various devices, charge transport is directly related to supramolecular order in fullerene systems. For example, Torres et al. observed high conductivity in self-assembled fullerene nanofibers deposited by drop-cast as opposed to spin-cast.³⁵ In this work, the conductivity of the fullerene-based mixtures was investigated with a bottom-gate, top-contact FET device configuration (Figure 3a), where divinyltetramethyldisiloxane bis(benzocyclobutene) (BCB)

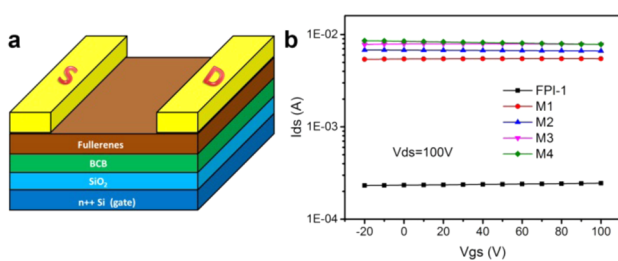


Figure 3. (a) FET device configuration. (b) I_{ds} vs V_{gs} plot for the films of pure FPI and the mixtures.

was thermally cross-linked before the spin-coating of fullerene materials. To the best of our knowledge, this is the first example of processing unfunctionalized fullerene and metallofullerene in an alcohol solvent. Like pure FPI-1,²⁷ all fullerene mixtures display conductive properties as the I_{ds} values are independent of gate voltage (Figures S4–S7). More importantly, all mixture films show significantly improved current compared to pure FPI (Figure 3b). The FPI-1 film exhibits a conductivity of 0.025 S/cm, consistent with our previous report.²⁷ With much higher currents, the mixtures M1, M2, M3, and M4 show 1 order of magnitude higher conductivities of 0.46 ± 0.07 , 0.54 ± 0.14 , 0.63 ± 0.09 , and 0.68 ± 0.12 S/cm, respectively. In a conductor, conductivity is determined by $\sigma = n \cdot q \cdot \mu$, where n is charge density, q is elementary charge, and μ is carrier mobility. In our system, we suggest the major contribution to the increased conductivity is from significantly enhanced carrier mobility (μ) due to tighter and ordered crystalline structure of the fullerene cages in the co-assemblies.^{11,36,37} That said, M2 shows higher conductivity than M1 which is consistent with its slightly tighter packing *vide supra* (Figure 2g). In M3 and M4 the intact fullerene or metallofullerene cage can contribute to

higher charge mobility, as evidenced by their higher conductivity values. Interestingly, M4 edges out M3 in conductivity, which implies that the negative C_{80}^{6-} cage may slightly enrich the charge density (n) of the system.

In conclusion, we have described the co-assemblies of an amphiphilic fullerene derivative and a series of insoluble fullerene-based molecules into large crystalline domains and demonstrated corresponding film fabrication by simple spin-coating. These co-assemblies maintain conductive property in the FPI molecules while adopt the tight packing as in pristine fullerenes or small fullerene derivatives. Furthermore, our approach is generally applicable to diversified versions of insoluble fullerenes with profound difference in size, shape, and electronic properties. This will allow the tuning of nanoscale parameters to optimize the macroscopic behavior. Our work also provides a general approach to process insoluble conjugated molecules in eco-friendly and biocompatible solvents like alcohols and water. As applications of supramolecular fullerene assemblies are actively sought in various devices, we believe the concept illustrated by our work adds an important element to the molecular design and device development of functional conjugated molecules.

■ ASSOCIATED CONTENT

Supporting Information

Detailed information for materials, instruments, procedures, and supplementary figures. This material is available free of charge via the Internet at <http://pubs.acs.org>.

■ AUTHOR INFORMATION

Corresponding Author

*ajen@u.washington.edu

Notes

The authors declare no competing financial interest.

■ ACKNOWLEDGMENTS

We acknowledge the Air Force Office of Scientific Research (FA9550-09-1-0426), the Asian Office of Aerospace R&D (FA2386-11-1-4072), the Office of Naval Research (no. N00014-14-1-0170), the National Science Foundation Graduate Research Fellowship Program (no. DGE-1256082), and the Boeing Foundation for financial support. Part of this work was conducted at the University of Washington Molecular Analysis Facility, a member of the NSF National Nanotechnology Infrastructure Network (NNIN).

■ REFERENCES

- (1) Kroto, H. W.; Heath, J. R.; O'Brien, S. C.; Curl, R. F.; Smalley, R. E. *Nature* **1985**, *318*, 162.
- (2) Popov, A. A.; Yang, S.; Dunsch, L. *Chem. Rev.* **2013**, *113*, 5989.
- (3) Guldi, D. M.; Illescas, B. M.; Atienza, C. M.; Wielopolski, M.; Martin, N. *Chem. Soc. Rev.* **2009**, *38*, 1587.
- (4) Pinzon, J. R.; Villalta-Cerdas, A.; Echegoyen, L. *Unimolecular and Supramolecular Electronics I*; Springer: Berlin, 2012, 127.
- (5) Li, C.-Z.; Yip, H.-L.; Jen, A. K. Y. *J. Mater. Chem.* **2012**, *22*, 4161.
- (6) Hummelen, J. C.; Knight, B. W.; LePeq, F.; Wudl, F.; Yao, J.; Wilkins, C. L. *J. Org. Chem.* **1995**, *60*, 532.
- (7) Wienk, M. M.; Kroon, J. M.; Verhees, W. J. H.; Knol, J.; Hummelen, J. C.; van Hal, P. A.; Janssen, R. A. J. *Angew. Chem. Int. Ed.* **2003**, *42*, 3371.
- (8) Ross, R. B.; Cardona, C. M.; Guldi, D. M.; Sankaranarayanan, S. G.; Reese, M. O.; Kopidakis, N.; Peet, J.; Walker, B.; Bazan, G. C.; Van Keuren, E.; Holloway, B. C.; Drees, M. *Nat. Mater.* **2009**, *8*, 208.
- (9) Henson, Z. B.; Müllen, K.; Bazan, G. C. *Nat. Chem.* **2012**, *4*, 699.

- (10) Diao, Y.; Shaw, L.; Bao, Z.; Mannsfeld, S. C. B. *Energy Environ. Sci.* **2014**, *7*, 2145.
- (11) Li, H.; Tee, B. C. K.; Cha, J. J.; Cui, Y.; Chung, J. W.; Lee, S. Y.; Bao, Z. *J. Am. Chem. Soc.* **2012**, *134*, 2760.
- (12) Wei, L.; Yao, J.; Fu, H. *ACS Nano* **2013**, *7*, 7573.
- (13) Sawamura, M.; Kawai, K.; Matsuo, Y.; Kanie, K.; Kato, T.; Nakamura, E. *Nature* **2002**, *419*, 702.
- (14) Li, C.-Z.; Matsuo, Y.; Nakamura, E. *J. Am. Chem. Soc.* **2009**, *131*, 17058.
- (15) Li, C.-Z.; Matsuo, Y.; Nakamura, E. *J. Am. Chem. Soc.* **2010**, *132*, 15514.
- (16) Wessendorf, F.; Grimm, B.; Guldi, D. M.; Hirsch, A. *J. Am. Chem. Soc.* **2010**, *132*, 10786.
- (17) Lacher, S.; Matsuo, Y.; Nakamura, E. *J. Am. Chem. Soc.* **2011**, *133*, 16997.
- (18) Bottari, G.; de la Torre, G.; Guldi, D. M.; Torres, T. *Chem. Rev.* **2010**, *110*, 6768.
- (19) Babu, S. S.; Mohwald, H.; Nakanishi, T. *Chem. Soc. Rev.* **2010**, *39*, 4021.
- (20) Bottari, G.; Trukhina, O.; Ince, M.; Torres, T. *Coord. Chem. Rev.* **2012**, *256*, 2453.
- (21) Shrestha, L. K.; Ji, Q.; Mori, T.; Miyazawa, K. i.; Yamauchi, Y.; Hill, J. P.; Ariga, K. *Chem.—Asian J.* **2013**, *8*, 1662.
- (22) Shen, Y.; Nakanishi, T. *Phys. Chem. Chem. Phys.* **2014**, *16*, 7199.
- (23) Hollamby, M. J.; Karny, M.; Bomans, P. H. H.; Sommerdijk, N. A. J. M.; Saeki, A.; Seki, S.; Minamikawa, H.; Grillo, I.; Pauw, B. R.; Brown, P.; Eastoe, J.; Möhwald, H.; Nakanishi, T. *Nat. Chem.* **2014**, *6*, 690.
- (24) Nakamura, E.; Isobe, H. *Acc. Chem. Res.* **2003**, *36*, 807.
- (25) Li, C.-Z.; Chueh, C.-C.; Yip, H.-L.; O'Malley, K. M.; Chen, W.-C.; Jen, A. K. Y. *J. Mater. Chem.* **2012**, *22*, 8574.
- (26) Stevenson, S.; Rice, G.; Glass, T.; Harich, K.; Cromer, F.; Jordan, M. R.; Craft, J.; Hadju, E.; Bible, R.; Olmstead, M. M.; Maitra, K.; Fisher, A. J.; Balch, A. L.; Dorn, H. C. *Nature* **1999**, *401*, 55.
- (27) Li, C.-Z.; Chueh, C.-C.; Yip, H.-L.; Ding, F.; Li, X.; Jen, A. K. Y. *Adv. Mater.* **2013**, *25*, 2457.
- (28) Prato, M.; Maggini, M. *Acc. Chem. Res.* **1998**, *31*, 519.
- (29) Cassell, A. M.; Asplund, C. L.; Tour, J. M. *Angew. Chem., Int. Ed.* **1999**, *38*, 2403.
- (30) Guldi, D. M.; Gouloumis, A.; Vázquez, P.; Torres, T.; Georgakilas, V.; Prato, M. *J. Am. Chem. Soc.* **2005**, *127*, 5811.
- (31) Yamamoto, Y.; Zhang, G.; Jin, W.; Fukushima, T.; Ishii, N.; Saeki, A.; Seki, S.; Tagawa, S.; Minari, T.; Tsukagoshi, K.; Aida, T. *Proc. Nat. Acad. Sci. U. S. A.* **2009**, *106*, 21051.
- (32) Muñoz, A.; Illescas, B. M.; Sánchez-Navarro, M.; Rojo, J.; Martín, N. *J. Am. Chem. Soc.* **2011**, *133*, 16758.
- (33) Zhang, X.; Hsu, C.-H.; Ren, X.; Gu, Y.; Song, B.; Sun, H.-J.; Yang, S.; Chen, E.; Tu, Y.; Li, X.; Yang, X.; Li, Y.; Zhu, X. *Angew. Chem., Int. Ed.* **2015**, *54*, 114.
- (34) Huffman, D. R. *Phys. Today* **1991**, *44*, 22.
- (35) Bottari, G.; Olea, D.; Gómez-Navarro, C.; Zamora, F.; Gómez-Herrero, J.; Torres, T. *Angew. Chem., Int. Ed.* **2008**, *47*, 2026.
- (36) Zhang, J.; Tan, J.; Ma, Z.; Xu, W.; Zhao, G.; Geng, H.; Di, C. a.; Hu, W.; Shuai, Z.; Singh, K.; Zhu, D. *J. Am. Chem. Soc.* **2013**, *135*, 558.
- (37) Li, H. Y.; Fan, C. C.; Vosgueritchian, M.; Tee, B. C. K.; Chen, H. Z. *J. Mater. Chem. C* **2014**, *2*, 3617.